

Lawrence Berkeley National Laboratory

LBL Publications

Title

Nanoscale insights into the structure of solution-processed graphene by x-ray scattering

Permalink

<https://escholarship.org/uc/item/2r33z0bg>

Journal

2D Materials, 10(1)

ISSN

2053-1583

Authors

Yan, Zhengyu
Guimarey, María JG
Parvez, Khaled
[et al.](#)

Publication Date

2023

DOI

10.1088/2053-1583/ac9b6f

Peer reviewed

ACCEPTED MANUSCRIPT • OPEN ACCESS

Nanoscale Insights into the Structure of Solution-processed Graphene by X-ray scattering

To cite this article before publication: Zhengyu Yan *et al* 2022 *2D Mater.* in press <https://doi.org/10.1088/2053-1583/ac9b6f>

Manuscript version: Accepted Manuscript

Accepted Manuscript is “the version of the article accepted for publication including all changes made as a result of the peer review process, and which may also include the addition to the article by IOP Publishing of a header, an article ID, a cover sheet and/or an ‘Accepted Manuscript’ watermark, but excluding any other editing, typesetting or other changes made by IOP Publishing and/or its licensors”

This Accepted Manuscript is © 2022 The Author(s). Published by IOP Publishing Ltd..

As the Version of Record of this article is going to be / has been published on a gold open access basis under a CC BY 3.0 licence, this Accepted Manuscript is available for reuse under a CC BY 3.0 licence immediately.

Everyone is permitted to use all or part of the original content in this article, provided that they adhere to all the terms of the licence <https://creativecommons.org/licenses/by/3.0>

Although reasonable endeavours have been taken to obtain all necessary permissions from third parties to include their copyrighted content within this article, their full citation and copyright line may not be present in this Accepted Manuscript version. Before using any content from this article, please refer to the Version of Record on IOPscience once published for full citation and copyright details, as permissions may be required. All third party content is fully copyright protected and is not published on a gold open access basis under a CC BY licence, unless that is specifically stated in the figure caption in the Version of Record.

View the [article online](#) for updates and enhancements.

Nanoscale Insights into the Structure of Solution-processed Graphene by X-ray scattering

Zhengyu Yan¹, María J. G. Guimarey^{2,3}, Khaled Parvez⁴, Chaochao Dun⁵, Oliver Read⁴,
Thomas Forrest⁶, Jeffrey J. Urban⁵, Amor Abdelkader², Cinzia Casiraghi⁴,
Wajira Mirihanage^{1, *}

¹Department of Material, University of Manchester, Manchester M13 9PL, UK

²Department of Engineering Bournemouth University, Poole BH12 5BB, UK

³Nafomat Group, Department of Applied Physics, University of Santiago de Compostela, 15782, Santiago de Compostela, Spain

⁴Department of Chemistry, University of Manchester, Manchester M13 9PL, UK

⁵The Molecular Foundry, Lawrence Berkeley National Laboratory, Berkley 94720, USA

⁶Diamond light source, Didcot, OX11 0DE, UK

Abstract

Chemical exfoliation is an attractive approach for the synthesis of graphene due to low cost and simplicity. However, challenges still remain in the characterization of solution-processed graphene, in particular with atomic resolution. Through this work we demonstrate the X-ray pair distribution function as a novel approach to study the solution-processed graphene or other 2D materials with atomic resolution, directly in solution, produced by liquid-phase and electrochemical exfoliations. The results show the disappearance of long-range atomic correlations, in both cases, confirming the production of single and few-layer graphene. In addition, a considerable ring distortion

1
2
3 has been observed as compared to graphite, irrespective of the solvent used: the normal
4
5
6 surface angle to the sheet of the powder sample should be less than 6° , compatible with
7
8
9 ripples formation observed in suspended graphene. We attribute this effect to the
10
11
12 interaction of solvent molecules with the graphene nanosheets.
13
14
15
16
17
18
19

20 **KEYWORDS:** *Solution-processed graphene, X-ray Pair Distribution Function, atomic*
21
22 *structure*
23
24
25
26
27
28
29
30
31
32
33
34
35
36
37
38
39
40
41
42
43
44
45
46
47
48
49
50
51
52
53
54
55
56
57
58
59
60

Introduction

One of the most attractive and industrially scalable methods for graphene production is given by chemical exfoliation of graphite [1]–[4]. This approach gives rise to graphene dispersions, which can be further processed with simple and low-cost methods such as drop casting and inkjet printing [5]–[8]. The most used chemical exfoliation approaches are Liquid Phase Exfoliation (LPE) and Electrochemical Exfoliation (EC). The LPE method relies on the use of ultrasound and/or shear force to exfoliate bulk graphite into graphene suspended in a suitable solvent, such as N-Methyl-2-pyrrolidone (NMP), N,N-dimethylformamide (DMF), and Cyrene (Cy) [9]–[11]. The EC process is based on expanding the graphite layers following the intercalation of ions and small molecules driven by an external electric field. According to the charge of the intercalated ions, the graphite electrode works as an anode or cathode, hosting oxidation or reduction reactions, respectively [12]–[14]. Cathodic EC gives rise to defect-free graphene, but exfoliation does require several hours [15], [16], while anodic EC is quick but gives rise to slightly oxidised graphene [14].

Despite the use of simple methods to produce solution-processed graphene, its characterisation is very challenging because the nanosheets come in different sizes,

1
2
3 thicknesses and chemical functionalisation [10]. In addition, the lack of metrology
4
5
6 standards strongly limits the commercialisation of graphene-based products [10], [17],
7
8 [18]. Only recently, the community has defined some guidelines for the characterisation
9
10 of graphene-based materials [19], which led to the development of the first ISO/IEC
11
12 standard (ISO/TS 21356-1:2021) for measuring the structural properties of graphene
13
14 [20]. In particular, information on the atomic structure of solution-processed graphene is
15
16 currently provided by Transmission Electron Microscopy, which requires specific
17
18 sample preparation, and it is time-consuming, so it can only be performed on a selected
19
20 number of nanosheets. The electron beam can also damage or change the structure of the
21
22 nanosheets.
23
24
25
26
27
28
29
30
31

32
33 Synchrotron X-ray based characterisation techniques are increasingly employed in
34
35 material science [21]–[24] because of their high photon energy (shorter wavelengths),
36
37 increased penetration, and short measuring time due to the appreciable photon flux,
38
39 hence providing an elegant solution for materials characterisation. In particular, the X-
40
41 ray pair distribution function (XPDF) [24] can provide quantitative information on the
42
43 crystal structure, e.g., the average distances between the neighbouring atoms, enabling
44
45 insights into the material structure with nanoscale resolution. Nevertheless, to the best of
46
47 our knowledge, these types of measurements have been rarely performed on graphene-
48
49
50
51
52
53
54
55
56
57
58
59
60

1
2
3 based materials. Previous studies with high energy X-rays [25]–[28] focussed on the
4
5
6 study of various types of graphitic carbons, including graphene oxide, specifically with
7
8
9 the aim to identify the type of defects.
10

11
12
13 Herein, we applied the XPDF to the characterisation of solution-processed graphene
14
15
16 produced by LPE and EC and dispersed in different solvents. The geometrical
17
18
19 arrangement of carbon atoms in the ring has been obtained from the analysis of the
20
21
22 XPDF data. We observe structural deformations of the hexagonal carbon ring, compared
23
24
25 to the perfect planar geometry, inducing possible rippling at the scale of the inter-atomic
26
27
28 distances, which could be related to the interaction with the solvent molecules, as
29
30
31 predicted theoretically.
32
33
34
35
36
37
38
39
40
41

42 **Results and Discussion**

43
44
45 Solution-processed graphene was produced by using cathodic EC and LPE methods, as
46
47
48 outlined in Fig. 1 a) and b), (and supplementary Fig. S1.a) following the approaches
49
50
51 reported previously [12], [29]–[31]. The solution process samples contained either NMP
52
53
54 and Cy are named as Gr LPE(NMP) Gr LPE(Cy), Gr EC(NMP) and Gr EC(Cy)
55
56
57 (chemical structure of Cy is shown supplementary Fig. S1.b). The measurements were
58
59
60

performed directly in solution. In the case of EC graphene, the expanded graphite powder (EC powder) was also collected and measured in solid form. Commercially available graphite was also measured as a reference. The graphene concentration is determined by UV-vis spectroscopy using an absorption coefficient of $2207 \text{ L g}^{-1} \text{ m}^{-1}$ [32] and $2460 \text{ L g}^{-1} \text{ m}^{-1}$ [11] for EC and LPE graphene, respectively, measured at 660 nm. The concentrations are reported in Table S1, in the supplementary Information.

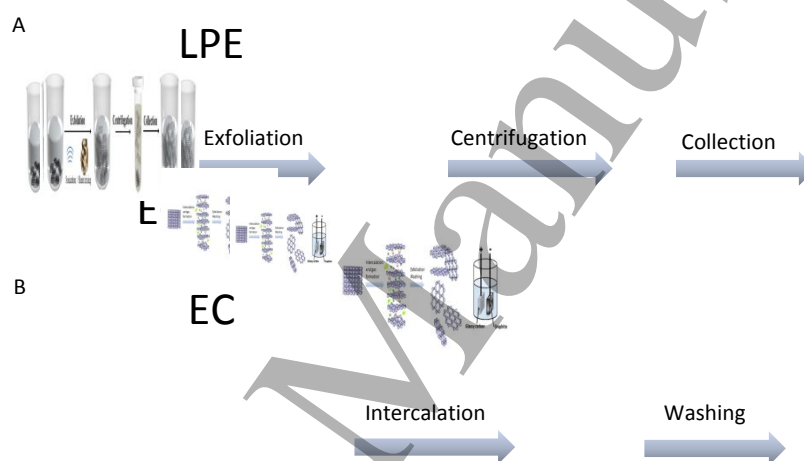


Figure 1: Schematic illustration of the exfoliation process: (a) Sonication-aided LPE process followed by centrifugation; (b) EC process using graphite as cathodic electrode.

The graphene nanosheets have been characterised by atomic force microscopy (AFM), Raman spectroscopy, high resolution transmission electron microscopy (HRTEM) and X-ray photoelectron spectroscopy (XPS). The thickness and lateral size distributions of

1
2
3 both LPE and EC graphene flakes were estimated by AFM (Fig. 2A and D). Fig. 2B and
4
5
6 E shows the statistics of the peak thickness of the LPE and EC graphene, respectively;
7
8
9 extracted from AFM over 300 individual flakes, revealing that the dispersions are
10
11
12 mostly composed of thin (<10 layers) graphene flakes. The lateral size distribution of
13
14
15 LPE and EC graphene in Fig. 2C and F, respectively, shows that the as-prepared
16
17
18 graphene nanosheets follows a broad distribution in size, where the average lateral size
19
20
21 for the LPE Gr was ~223 nm and between 1 – 4 μm for the EC Gr. The smaller flake
22
23
24 size for the LPE Gr compared to the EC Gr is due to the extensive sonication during the
25
26
27 exfoliation process and is in good agreement with our previous reports [7, 12]. Fig. 2G
28
29
30 and H shows representative Raman spectra measured on individual flakes produced by
31
32
33 LPE and EC, respectively. The typical Raman spectrum of LPE and EC Gr shows the D
34
35
36 and G peaks at $\sim 1350\text{ cm}^{-1}$ and $\sim 1580\text{ cm}^{-1}$, respectively [33]. The D peak is activated
37
38
39 by defects, but the specific activation mechanism is different between the two samples.
40
41
42 In the case of graphene produced by LPE, the D peak is activated by the edges of the
43
44
45 nanosheets, having lateral size comparable or smaller than that of the laser spot size [34].
46
47
48 The D peak in the Raman spectrum of EC graphene (Fig. 2H) is likely activated by
49
50
51 introducing functional groups during the electrochemical treatment, as evidenced by the
52
53
54
55
56
57
58
59
60

1
2
3 XPS results. It should also be noted that the gas bubbles collapse on the electrodes could
4
5
6 form different kinds of defects in the graphene basal plane, including generating some
7
8
9 vacancies. These defects could also be a result of structural defects introduced by the gas
10
11
12 evolution between the layers caused by the repeated ion intercalation/deintercalation
13
14
15
16 process during the exfoliation process.
17
18
19
20
21
22
23
24
25
26
27
28
29
30
31
32
33
34
35
36
37
38
39
40
41
42
43
44
45
46
47
48
49
50
51
52
53
54
55
56
57
58
59
60

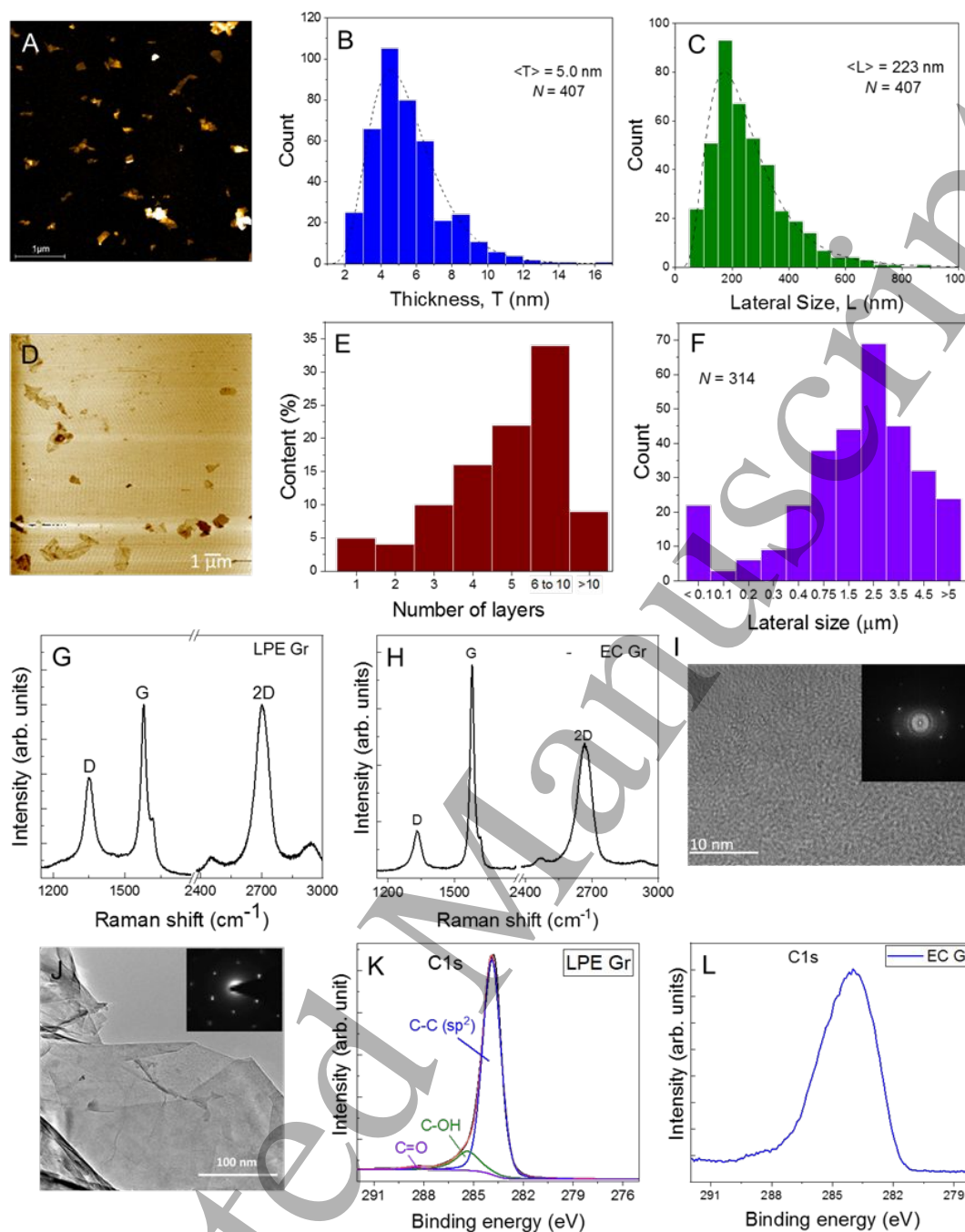


Figure 2: (A) Typical AFM image of LPE graphene drop-casted on SiO₂/Si substrate; (B) thickness and (C) lateral size distribution of LPE graphene measured by AFM; (D) typical AFM image of EC graphene; (E) number of layers and (F) lateral size distribution of EC graphene measured by AFM; (G) and (H) representative Raman spectra of LPE and EG graphene measured with 514.5 nm

1
2
3 High resolution TEM (HRTEM) images reveal that the graphene nanosheets produced
4
5
6 by the LPE and EC processes are clean and high crystallinity. Moreover, both the FFT
7
8
9 and SAED patterns of LPE and EC graphene (inset of Fig. 2I and J, respectively) reveals
10
11
12 the bright inner ring of {0-110} spots and faint outer ring of {1-210} spots, revealing the
13
14
15 typical diffraction pattern of monolayer graphene. Moreover, the High-Angle Annular
16
17
18 Dark Field (HAADF) and the corresponding Energy Disperse Spectroscopy (EDS)
19
20
21 mapping of the graphene flake (supplementary Fig. S2) demonstrates the graphene
22
23
24 produced by the LPE process consists of pristine flakes without any impurities.
25
26
27

28
29
30 The chemical composition of the as-prepared graphene was further investigated by the
31
32
33 XPS. As shown in Fig. 2 J and K, both the XPS spectra of the LPE and EC graphene
34
35
36 show asymmetric C1s peak centred ~284 eV corresponding to sp^2 C-C bond. Noticeably,
37
38
39 only a tiny amount of oxygen related functional groups (i.e. C-OH and C=O groups at
40
41
42 285.5 eV and 288.4 eV, respectively) were observed in LPE Gr, which mainly inherited
43
44
45 form the starting graphite used for the exfoliation process [35] . On the other hand, the
46
47
48 oxygen content of the EC Gr was found to be around 7.8 at% compared to the 5.5 at% of
49
50
51 pure graphite (supplementary Figs. S3 and Fig.S4), supporting the assumption the EC
52
53
54
55
56
57
58
59
60 exfoliation process used is largely nonoxidative. Therefore, both the LPE and EC Gr

1
2
3 used in this study are of high quality and crystallinity as supported by different
4
5
6 characterization methods discussed above.
7
8
9

10 For X-ray characterization, the samples were packed in a borosilicate capillary with 1.5
11
12 mm diameter. The background signal measurement is conducted, (as shown in
13
14 supplementary Fig. S5) and subtracted from the signal of the graphene. As shown in Fig.
15
16
17 3A, during the synchrotron X-ray experiments, the capillaries are mounted horizontally
18
19
20 and rotated about its long axis centring the X-ray beam at the upper half of the capillary
21
22
23 to avoid any precipitations of the highly concentrated solution sample. The exposure
24
25
26 time for each X-ray scattering measurement was 300 s. The experimentally collected
27
28
29 diffraction intensity data, including Bragg's scattering signal and high Q range scattering
30
31
32 signal can be primarily processed into the total scattering structure function, $S(Q)$,
33
34 representing the normalised scattering cross-section form [21]. A highly monochromatic
35
36
37 synchrotron X-ray beam was used; hence zero bremsstrahlung contribution can be
38
39
40 assumed. The top-hat width for the Lorch function of 1.0 \AA^{-1} was utilised, and a
41
42
43 minimum Fourier filter radius of 1.25 \AA^{-1} was used for the Fourier transform.
44
45
46
47
48
49
50
51

52
53
54 Fig. 3B shows the $S(Q)$ of all the samples with subtraction of the background. In the
55
56
57 case of graphite, the intense peak-like features are characteristic of a 3-dimensional and
58
59
60

1
2
3 highly crystalline structure. In the case of EC powder, the peaks over $Q = 3 \text{ \AA}^{-1}$ decrease
4
5
6 in intensity, while the intensity of the peak just below $Q = 2 \text{ \AA}^{-1}$ increases. The solution-
7
8
9 processed graphene obtained by LPE and by cathodic EC show a similar spectrum,
10
11
12 characterised by a broad peak at about $Q = 1.1 \text{ \AA}^{-1}$. The missing/decreased intensity of
13
14
15 the peaks is related to a change in structure, associated with a reduced ordered
16
17
18 configuration of the atoms. The processed XPDF spectra up to 25 \AA is shown in Fig. 3C.
19
20
21 Graphite shows obvious atomic correlations up to 15 \AA or more. In the case of the
22
23
24 graphite powder, the correlation is visible up to 10 \AA . On the other hand, in the case of
25
26
27 solution-processed graphene, long-distance correlations are completely missing. The
28
29
30 absence of long-distance correlation peaks indicates the disappearance of the three-
31
32
33 dimensional (3D) structure due to the exfoliation (as in the case of LPE and EC samples).
34
35
36
37 The exfoliation caused lack of repeated atomic correlation between the layers of graphite
38
39
40 (i.e., loss of AB-stacking), as in the case of the EC powder.
41
42
43
44
45
46
47
48
49
50
51
52
53
54
55
56
57
58
59
60

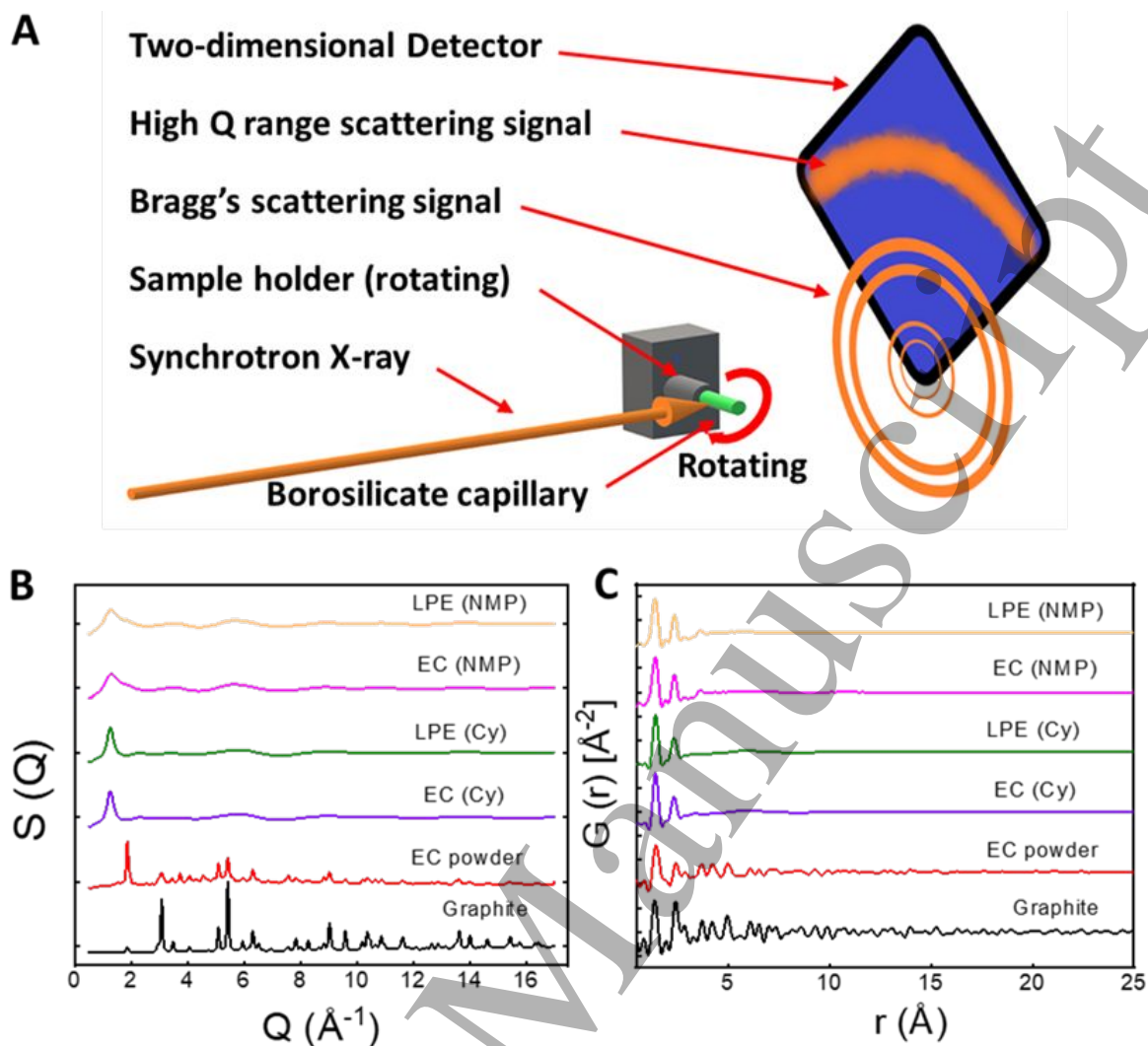


Figure 3: (a) Schematic illustration of the synchrotron x-ray experiment set up with 2D area detector; (b) Structure factor results calculated from the collected diffraction intensity; (c) XPDF results of LPE, EC exfoliated graphene and Bulk graphite

In the case of solution-processed graphene, only the two peaks at short correlation distances ($< 5 \text{\AA}$) are clearly visible. However, a closer look in this region, Fig. 4A, shows that the number of peaks and their positions is slightly different, depending on the

1
2
3 sample considered. These peaks are very important because their position is associated
4
5
6 with the C-C atomic distance in the ring: by using the carbon hexagon model from
7
8
9 graphite in Fig. 4B, one would expect to see 5 peaks at the distances 1.41 Å, 2.42 Å,
10
11
12 2.86 Å, 3.74 Å, 4.22 Å, corresponding to the C1-C2, C1-C3, C1-C4, C1-C5, C1-C6
13
14
15 atomic distances, respectively. This is well observed with the selected Q range of XPDF
16
17
18 spectrum, as shown in Fig. 4A, which also agrees with the previous research [36], [37].
19
20
21

22
23 Fig. 4C shows that the C1-C2 bonding in graphite powder increases up to 1.46 Å, while
24
25
26 it is fixed at 1.43 Å or 1.44 Å for solution-processed graphene, irrespective of the
27
28
29 exfoliation method used. Note that cathodic graphene has a size comparable to graphene
30
31
32 flakes made by LPE [12]. The C1-C3 distance slightly increases in graphite powder
33
34
35 compared to bulk graphite, while it is much smaller in the case of solution-processed
36
37
38 graphene. The same is observed for C1-C4, although the signal of solution-processed
39
40
41 graphene is rather weak with a broad peak but can still be recognised at about 2.85 Å,
42
43
44 which indicates that the C1-C4 atomic correlation is hardly visible measured as a fixed
45
46
47 value. In the case of the C1-C5 distance, no significant differences are observed between
48
49
50 bulk graphite and EC graphite powder. In contrast, the C1-C5 distances are reduced in
51
52
53 the case of solution-processed graphene, with no dependence on the exfoliation method.
54
55
56
57
58
59
60

1
2
3 The peak associated with C1-C6 is missing in the case of solution-processed graphene.
4
5

6 The correlation of longer distance C1-C6 becomes too weak to be detected by the XPDF,
7
8
9 which can be regarded as uncorrelated pair.
10
11
12

13 Interestingly, any correlation associated with NMP or Cyrene (for structure details
14
15 readers are referred to ref. [29]) is not observed in solution-processed graphene. The
16
17 intermolecular correlation of the solvent molecules could be visible if the molecules are
18
19 ordered in space. However, the NMP and Cyrene molecules are probably randomly
20
21 spaced with relatively low concentration, which means no constructive scattering can
22
23 occur even without removing the background. Therefore, all of the characteristic peaks
24
25 of the solvent molecules are not observed in our spectra. All the correlation peaks, and
26
27 in particular the one at 1.43-1.44 Å for solution-processed graphene, are doubtlessly
28
29 coming from graphene. Thus, the difference between graphene in NMP and Cyrene is
30
31 minimal and can be neglected [29].
32
33
34
35
36
37
38
39
40
41
42
43
44
45
46
47
48
49
50
51
52
53
54
55
56
57
58
59
60

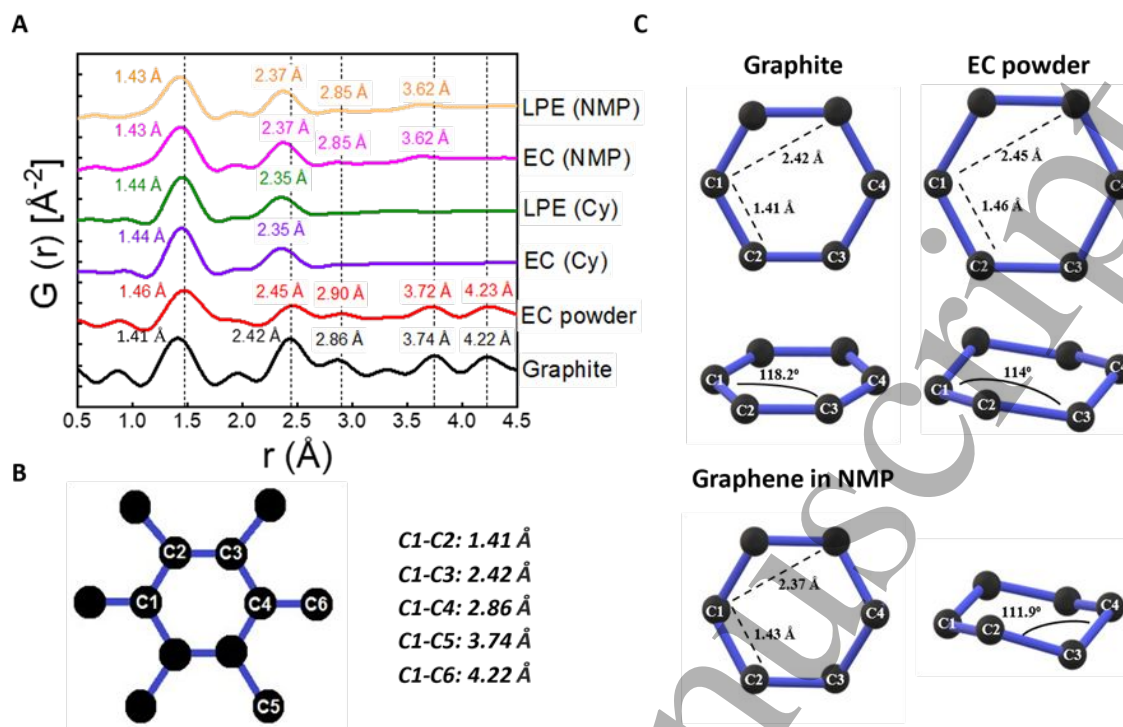


Figure 4: (a) XPDF results of a carbon hexagon range up to 4.5 \AA ; (b) Carbon hexagon model from graphite. Distances between atoms are noted; (c) Carbon hexagon models with distortion of single layer graphene in bulk graphite, EC expanded graphite powder, graphene

The XPDF results confirm that cathodic EC and LPE can provide nanosheets with thickness small enough to be considered 2-dimensional. However, slightly different geometric arrangements of the atoms in the hexagonal ring have been observed as compared to graphite. Fig. 4 c) shows the resulting carbon hexagon models for solution-processed graphene in NMP and EC graphite powder compared to that of graphite. Our results show that ion intercalation and related layers' expansion, caused by the cathodic

1
2
3 EC process, gives rise to a small ring distortion compared to pristine graphene. However,
4
5
6 the ring distortion further increases when the material is dispersed in a solvent.
7
8
9 Remarkably, as both LPE and EC graphene dispersed in the same solvent show exactly
10
11
12 the same type of distortion of the hexagonal ring, this effect is likely to be caused by the
13
14
15 interaction between solvent molecules and graphene. Nevertheless, careful further
16
17
18 research needs to be drawing any such conclusions beyond the doubts. In such case,
19
20
21
22
23 XPDF can emerge as one the key technique that can be providing valuable experimental
24
25
26 measurements.

27
28
29 Remarkably, Meyer et al. [38] have suggested ripples in suspended graphene through
30
31
32 TEM investigations, as confirmed by other groups [39]–[41]. In particular, an average of
33
34
35 0.7 Å height fluctuation (i.e. ripple height normal to the sheet) was found by using
36
37
38 Monte Carlo simulation [42]. The bond length deviation is predicted from 1.31 Å to
39
40
41 1.54 Å. This could include the short double bond of 1.31 Å, a conjugated bond of 1.42 Å,
42
43
44 and up to a long single bond of 1.54 Å. Hence, the three bonds of each carbon atom
45
46
47 within the hexagon could be different. Our results show ring distortions compatible with
48
49
50 the proposed model for suspended graphene [39]; as the C1-C3 atomic distance of
51
52
53 solution-processed graphene becomes shorter than the bulk graphite. However, it needs
54
55
56
57
58
59
60

1
2
3 to be noted that TEM measurements were done on the suspended graphene while our
4
5
6 measurements details were here obtained while the graphene in solution, where we
7
8
9 found some indications for influence the distortion. The increasing bond lengths
10
11
12 differences indicate that the graphene's increased density is not perfectly planar when
13
14
15 dispersed in a solvent. The bonding angle between C1-C2-C3 is calculated as 111.9° and
16
17
18 114° for graphene dispersion and powder. The normal surface angle to the sheet of the
19
20
21 powder sample should be less than 6° (i.e. the angle deviation of 114° from 120°), and
22
23
24 this result is consistent with the angle deviation of the result from Meyer's result [38],
25
26
27 where the angle deviation from the sheet is $\pm 5^\circ$. Likely, this effect is caused by the
28
29
30 specific interaction of the solvent with graphene.
31
32
33
34
35
36

37 **Conclusions**

38
39
40 Our work presents the first characterisation of solution-processed graphene in NMP and
41
42
43 Cyrene by high energy X-ray scattering and related XPDF analysis. The results show the
44
45
46 disappearance of long-range atomic correlations, confirming the production of 2D
47
48
49 nanosheets and that the hexagonal atomic structure is strongly distorted when graphene
50
51
52 is suspended in a medium. In particular, the first C-C distance slightly increases, while
53
54
55 the second C-C distance decreases, resulting in a distortion that could be compatible
56
57
58
59
60

1
2
3 with ripples formation observed in suspended graphene, likely to be caused by the
4
5
6 interaction of solvent molecules with the graphene nanosheets. Our results demonstrate
7
8
9 the potential of XPDF as a powerful tool to characterise 2D materials and acquire
10
11
12 quantitative structural information with atomic resolution.
13
14
15
16
17
18

19 **Methods**

20
21
22 **Materials.** High purity graphite foil (99.8% metal basis), graphite rod (99.99% metal
23
24
25 basis) and ammonium sulfate ((NH₄)₂SO₄, 98+%) were purchased from Alfa Aesar.
26
27
28 Anhydrous dimethyl sulfoxide (DMSO) (99.9%), graphite flakes (100+ mesh), 1-
29
30
31 Pyrenesulfonic acid sodium salt (PS1) and isopropyl alcohol (IPA) were purchased from
32
33
34 Sigma-Aldrich. Isomolded graphite (>99.95%) rods were purchased from GraphiteStore.
35
36
37 Cesium perchlorate (99%) was obtained from Fisher Scientific. The natural kish graphite
38
39
40 was bought from Graphexel Ltd. All the chemicals and materials were used as received.
41
42
43
44
45

46
47 **Exfoliation.** The LPE graphene in NMP was prepared by adding 300 mg of graphite
48
49
50 flakes into 100 mL of NMP, followed by sonicating the mixture at 600 W using Hilsonic
51
52
53 bath sonicator for 5 days. Afterwards, the dispersion was centrifuged using a Sigma 1-
54
55
56 14k refrigerated centrifuge at 903g for 20 min to remove un-exfoliated graphite. To
57
58
59
60

1
2
3 obtain highly concentrated graphene, the dispersion was further centrifuged at 16600 g
4
5
6 for 1 hr., followed by re-dispersing the sedimented graphene into a small volume of
7
8
9 NMP. The EC is prepared by the cathodic electrochemical exfoliation as described in
10
11
12 our previous work [12]. Briefly, a pellet of natural graphite is used as a cathode, and Pt
13
14
15 mesh was used as the anode. The electrolyte was 1M lithium chloride (Sigma Aldrich,
16
17
18 99.9%), and Triethylamine hydrochloride in dimethyl sulfoxide. The exfoliation
19
20
21 products were washed to remove the electrolyte with water and ethanol until the pH was
22
23
24 neutral, and the products were separated by filtration using Anodisc alumina membranes
25
26
27 with 100 nm pore size and then dried at 200 °C under Ar atmosphere. The dry powder
28
29
30 was then dispersed in a small amount of NMA, as in the LPE samples.
31
32
33
34
35
36

37 **Materials characterization.** UV-Vis spectroscopy of the graphene dispersions were
38
39
40 measured by using a PerkinElmer I-900 UV-Vis-NIR spectrometer. A Bruker Atomic
41
42
43 Force Microscope (MultiMode 8) in Peak Force Tapping mode, equipped with
44
45
46 ScanAsyst-Air tips is used to determine the lateral size and thickness distribution of the
47
48
49 graphene flakes. The samples were prepared by drop casting the dispersion on a clean
50
51
52 silicon substrate; several hundreds of individual flakes were selected, after complete
53
54
55 solvent evaporation, for lateral size and thickness analysis. The same sample preparation
56
57
58
59
60

1
2
3 has been used for Raman measurements. Raman measurements were performed using a
4
5
6 Renishaw Invia Raman spectrometer equipped with a 514.5 nm excitation line with 1
7
8
9 mW laser power. 100X NA0.85 objective lens, giving a spatial resolution of ~500 nm,
10
11
12 and 2400 grooves/nm grating were used for the measurements. The X-ray photoelectron
13
14
15 spectroscopy (XPS) measurements were performed using the K-Alpha X-ray
16
17
18 Photoelectron Spectrometer (XPS) System from Thermo Scientific. The photon source
19
20
21 was a monochromatized Al K α line ($h\nu = 1486.6$ eV). The spectra were acquired using
22
23
24 a spot size of 300 μ m and constant pass energy (150 eV for survey and 20 eV for high
25
26
27 resolution spectra). A flood gun with combined electrons and low energy Ar ions is used
28
29
30 during the measurements. HRTEM images were acquired on a JEOL 2100-F microscope
31
32
33 with a field-emission gun operated at 200 kV accelerating voltage providing direct
34
35
36 images of the atomic structure. A High-Angle Annular Dark Field (HAADF) detector
37
38
39 and an Oxford high solid-angle Silicon Drift Detector (SDD) X-Ray Energy Dispersive
40
41
42 Spectrometer (EDS) system was used for chemical elemental analysis.
43
44
45
46
47

48
49
50 **X-Ray Scattering.** The synchrotron X-ray scattering experiments were conducted in I15-
51
52
53 1 beamline, Diamond Light Source, U.K. The monochromatic X-ray beam with 76.7
54
55
56 keV (wavelength of 0.161669 Å) was employed [43]. A 2D Perkin Elmer XRD detector
57
58
59
60

with active area of $409.6 \times 409.6 \text{ mm}^2$ and pixel size of $100 \mu\text{m}$ was applied close to sample to provide large Q range and high-quality scattering data. Here $Q = (4\pi \sin\theta)/\lambda$, where λ is the wavelength and 2θ is the angle between incident and scattered X-rays. The collected diffraction intensity data is processed by software GudrunX [44] which subtracts the self-scattering intensity, Compton scattering and multiple scattering, etc. Then, the total scattering structure factor, $S(Q)$ and X-ray pair distribution function (XPDF), $G(r)$ are obtained as;

$$S(Q) = \frac{I(Q)}{\langle b^2 \rangle} \quad (1)$$

$$G(r) = \frac{2}{\pi} \int_{Q_{\min}}^{Q_{\max}} Q [S(Q) - 1] \sin(Qr) dQ \quad (2)$$

where $I(Q)$ is the collected and processed diffraction intensity. The coherent single-scattering intensity is desired; b is the element scattering amplitude (f is used for x-ray scattering); $\langle \dots \rangle$ denotes an averaging process. For detailed theory, ref. [21], [45] is referred.

Acknowledgements

We acknowledged Diamond Light Source for granting beamtime at I15-1 (CY24816).

WM acknowledges the funding from EPSRC (UK) grant EP/P02680X/1. The work of MJGG is supported by the Xunta de Galicia (Spain) Postdoctoral Fellowship with reference ED481B-2019-015. CC and KP acknowledge the Graphene Flagship Core 3 (Contract No.881603) and the ERC Project PEP2P (Contract No. 770047). OR acknowledges financial support from the Lloyd's Register Foundation. CD and JU acknowledge the Office of Science, Office of Basic Energy Sciences, of the U.S. Department of Energy (Contract No. DE-AC02-05CH11231).

Author contributions

ZY, AA and WM conceived the approach and designed the experiments. AA, WM, and TF carried out the X-ray experiments while MG and KP prepared materials and carried out lab experiments. OR, CD and JU performed the material characterizations with AFM, HRTEM, EDS and XPS analysis. ZY performed the analysis the data and drafted the manuscript with inputs from CC, AA and WM. All authors discussed the results and contributed to the manuscript.

References

- [1] F. Bonaccorso, A. Bartolotta, J. N. Coleman, and C. Backes, '2D-Crystal-Based Functional Inks', *Adv. Mater.*, vol. 28, no. 29, pp. 6136–6166, 2016, doi: 10.1002/adma.201506410.
- [2] C. Backes *et al.*, 'Production and processing of graphene and related materials', *2D Mater.*, vol. 7, no. 2, p. 022001, Jan. 2020, doi: 10.1088/2053-1583/ab1e0a.
- [3] X. Cai, Y. Luo, B. Liu, and H.-M. Cheng, 'Preparation of 2D material dispersions and their applications', *Chem. Soc. Rev.*, vol. 47, no. 16, pp. 6224–6266, 2018, doi: 10.1039/C8CS00254A.
- [4] A. Ciesielski and P. Samorì, 'Graphene via sonication assisted liquid-phase exfoliation', *Chem Soc Rev*, vol. 43, no. 1, pp. 381–398, 2014, doi: 10.1039/C3CS60217F.
- [5] A. G. Kelly *et al.*, 'All-printed thin-film transistors from networks of liquid-exfoliated nanosheets', *Science*, vol. 356, no. 6333, pp. 69–73, Apr. 2017, doi: 10.1126/science.aal4062.
- [6] E. B. Secor and M. C. Hersam, 'Emerging Carbon and Post-Carbon Nanomaterial Inks for Printed Electronics', *J. Phys. Chem. Lett.*, vol. 6, no. 4, pp. 620–626, Feb. 2015, doi: 10.1021/jz502431r.
- [7] D. McManus *et al.*, 'Water-based and biocompatible 2D crystal inks for all-inkjet-printed heterostructures', *Nat. Nanotechnol.*, vol. 12, no. 4, pp. 343–350, Apr. 2017, doi: 10.1038/nnano.2016.281.
- [8] F. Torrìsi *et al.*, 'Inkjet-Printed Graphene Electronics', *ACS Nano*, vol. 6, no. 4, pp. 2992–3006, Apr. 2012, doi: 10.1021/nn2044609.
- [9] V. Nicolosi, M. Chhowalla, M. G. Kanatzidis, M. S. Strano, and J. N. Coleman, 'Liquid Exfoliation of Layered Materials', *Science*, vol. 340, no. 6139, pp. 1226419–1226419, Jun. 2013, doi: 10.1126/science.1226419.
- [10] C. Backes *et al.*, 'Guidelines for Exfoliation, Characterization and Processing of Layered Materials Produced by Liquid Exfoliation', *Chem. Mater.*, vol. 29, no. 1, pp. 243–255, Jan. 2017, doi: 10.1021/acs.chemmater.6b03335.
- [11] Y. Hernandez *et al.*, 'High-yield production of graphene by liquid-phase exfoliation of graphite', *Nat. Nanotechnol.*, vol. 3, no. 9, pp. 563–568, Sep. 2008,

- doi: 10.1038/nnano.2008.215.
- [12] A. M. Abdelkader, I. A. Kinloch, and R. A. W. Dryfe, 'Continuous Electrochemical Exfoliation of Micrometer-Sized Graphene Using Synergistic Ion Intercalations and Organic Solvents', *ACS Appl. Mater. Interfaces*, vol. 6, no. 3, pp. 1632–1639, Feb. 2014, doi: 10.1021/am404497n.
- [13] A. M. Abdelkader, 'Electrochemical synthesis of highly corrugated graphene sheets for high performance supercapacitors', *J. Mater. Chem. A*, vol. 3, no. 16, pp. 8519–8525, 2015, doi: 10.1039/C5TA00545K.
- [14] K. Parvez *et al.*, 'Exfoliation of Graphite into Graphene in Aqueous Solutions of Inorganic Salts', *J. Am. Chem. Soc.*, vol. 136, no. 16, pp. 6083–6091, Apr. 2014, doi: 10.1021/ja5017156.
- [15] A. J. Cooper, N. R. Wilson, I. A. Kinloch, and R. A. W. Dryfe, 'Single stage electrochemical exfoliation method for the production of few-layer graphene via intercalation of tetraalkylammonium cations', *Carbon*, vol. 66, pp. 340–350, Jan. 2014, doi: 10.1016/j.carbon.2013.09.009.
- [16] Y. Yang, F. Lu, Z. Zhou, W. Song, Q. Chen, and X. Ji, 'Electrochemically cathodic exfoliation of graphene sheets in room temperature ionic liquids N-butyl, methylpyrrolidinium bis(trifluoromethylsulfonyl)imide and their electrochemical properties', *Electrochimica Acta*, vol. 113, pp. 9–16, Dec. 2013, doi: 10.1016/j.electacta.2013.09.031.
- [17] P. Wick *et al.*, 'Classification Framework for Graphene-Based Materials', *Angew. Chem. Int. Ed.*, vol. 53, no. 30, pp. 7714–7718, Jul. 2014, doi: 10.1002/anie.201403335.
- [18] K. Kostarelos and K. S. Novoselov, 'Graphene devices for life', *Nat. Nanotechnol.*, vol. 9, no. 10, pp. 744–745, Oct. 2014, doi: 10.1038/nnano.2014.224.
- [19] A J Pollard *et al.*, 'Characterisation of the structure of graphene', *Characterisation of the structure of graphene*, 2017.
- [20] 'ISO/TS 21356-1:2021 Nanotechnologies — Structural characterization of graphene — Part 1: Graphene from powders and dispersions': [Online]. Available: <https://www.iso.org/standard/70757.html>
- [21] T. Egami and S. J. L. Billinge, Eds., *Underneath the Bragg Peaks Structural Analysis of Complex Materials*, vol. 16. Pergamon, 2012. doi: 10.1016/B978-0-08-097133-9.09994-9.
- [22] D. H. Bilderback, P. Elleaume, and E. Weckert, 'Review of third and next

- generation synchrotron light sources', *J. Phys. B At. Mol. Opt. Phys.*, vol. 38, no. 9, pp. S773–S797, May 2005, doi: 10.1088/0953-4075/38/9/022.
- [23] J. B. Hastings, W. Thomlinson, and D. E. Cox, 'Synchrotron X-ray powder diffraction', *J. Appl. Crystallogr.*, vol. 17, no. 2, pp. 85–95, 1984, doi: 10.1107/S0021889884011043.
- [24] M. W. Westneat, J. J. Socha, and W.-K. Lee, 'Advances in Biological Structure, Function, and Physiology Using Synchrotron X-Ray Imaging', *Annu. Rev. Physiol.*, vol. 70, no. 1, pp. 119–142, Mar. 2008, doi: 10.1146/annurev.physiol.70.113006.100434.
- [25] M. A. Smith, H. C. Foley, and R. F. Lobo, 'A simple model describes the PDF of a non-graphitising carbon', *Carbon*, vol. 42, no. 10, pp. 2041–2048, Jan. 2004, doi: 10.1016/j.carbon.2004.04.009.
- [26] V. Petkov, R. G. Difrancesco, S. J. L. Billinge, M. Acharya, and H. C. Foley, 'Local structure of nanoporous carbons', *Philos. Mag. B*, vol. 79, no. 10, pp. 1519–1530, Oct. 1999, doi: 10.1080/13642819908218319.
- [27] N. Woznica, L. Hawelek, H. E. Fischer, I. Bobrinetskiy, and A. Burian, 'The atomic scale structure of graphene powder studied by neutron and X-ray diffraction', *J. Appl. Crystallogr.*, vol. 48, no. 5, pp. 1429–1436, Oct. 2015, doi: 10.1107/S1600576715014053.
- [28] N. Woźnica *et al.*, 'The atomic scale structure of saccharose-based carbons', *Philos. Mag.*, vol. 97, no. 20, pp. 1675–1697, Jul. 2017, doi: 10.1080/14786435.2017.1313465.
- [29] H. J. Salavagione *et al.*, 'Identification of high performance solvents for the sustainable processing of graphene', *Green Chem.*, vol. 19, no. 11, pp. 2550–2560, 2017, doi: 10.1039/C7GC00112F.
- [30] J. N. Coleman, 'Liquid Exfoliation of Defect-Free Graphene', *Acc. Chem. Res.*, vol. 46, no. 1, pp. 14–22, Jan. 2013, doi: 10.1021/ar300009f.
- [31] J. Wang, K. K. Manga, Q. Bao, and K. P. Loh, 'High-Yield Synthesis of Few-Layer Graphene Flakes through Electrochemical Expansion of Graphite in Propylene Carbonate Electrolyte', *J. Am. Chem. Soc.*, vol. 133, no. 23, pp. 8888–8891, Jun. 2011, doi: 10.1021/ja203725d.
- [32] K. Parvez, R. Worsley, A. Alieva, A. Felten, and C. Casiraghi, 'Water-based and inkjet printable inks made by electrochemically exfoliated graphene', *Carbon*, vol. 149, pp. 213–221, Aug. 2019, doi: 10.1016/j.carbon.2019.04.047.

- 1
2
3 [33] V. Nagyte *et al.*, 'Raman Fingerprints of Graphene Produced by Anodic
4 Electrochemical Exfoliation', *Nano Lett.*, vol. 20, no. 5, pp. 3411–3419, May 2020,
5 doi: 10.1021/acs.nanolett.0c00332.
6
7
8 [34] C. Casiraghi *et al.*, 'Raman Spectroscopy of Graphene Edges', *Nano Lett.*, vol. 9,
9 no. 4, pp. 1433–1441, Apr. 2009, doi: 10.1021/nl8032697.
10
11 [35] N. G. Shang *et al.*, 'Controllable selective exfoliation of high-quality graphene
12 nanosheets and nanodots by ionic liquid assisted grinding', *Chem. Commun.*, vol. 48,
13 no. 13, p. 1877, 2012, doi: 10.1039/c2cc17185f.
14
15 [36] V. Petkov, Y. Ren, S. Kabekkodu, and D. Murphy, 'Atomic pair distribution
16 functions analysis of disordered low-Z materials', *Phys. Chem. Chem. Phys.*, vol. 15,
17 no. 22, p. 8544, 2013, doi: 10.1039/c2cp43378h.
18
19 [37] A. Burian, J. C. Dore, and K. Jurkiewicz, 'Structural studies of carbons by neutron
20 and x-ray scattering', *Rep. Prog. Phys.*, vol. 82, no. 1, p. 016501, Jan. 2019, doi:
21 10.1088/1361-6633/aae882.
22
23 [38] J. C. Meyer, A. K. Geim, M. I. Katsnelson, K. S. Novoselov, T. J. Booth, and S.
24 Roth, 'The structure of suspended graphene sheets', *Nature*, vol. 446, no. 7131, pp.
25 60–63, Mar. 2007, doi: 10.1038/nature05545.
26
27 [39] A. Amiri, M. Naraghi, G. Ahmadi, M. Soleymaniha, and M. Shanbedi, 'A review
28 on liquid-phase exfoliation for scalable production of pure graphene, wrinkled,
29 crumpled and functionalized graphene and challenges', *FlatChem*, vol. 8, pp. 40–71,
30 Mar. 2018, doi: 10.1016/j.flatc.2018.03.004.
31
32 [40] Z. Li *et al.*, 'Deformation of Wrinkled Graphene', *ACS Nano*, vol. 9, no. 4, pp.
33 3917–3925, Apr. 2015, doi: 10.1021/nm507202c.
34
35 [41] N. Liu, Z. Pan, L. Fu, C. Zhang, B. Dai, and Z. Liu, 'The origin of wrinkles on
36 transferred graphene', *Nano Res.*, vol. 4, no. 10, pp. 996–1004, Oct. 2011, doi:
37 10.1007/s12274-011-0156-3.
38
39 [42] A. Fasolino, J. H. Los, and M. I. Katsnelson, 'Intrinsic ripples in graphene', *Nat.*
40 *Mater.*, vol. 6, no. 11, pp. 858–861, Nov. 2007, doi: 10.1038/nmat2011.
41
42 [43] P. A. Chater, D. Keeble, M. Wharmby, T. Spain, J. Filik, and H. Wilhelm, 'The
43 automated XPDF beamline at Diamond Light Source', *Acta Crystallogr. Sect.*
44 *Found. Adv.*, vol. 73, no. a2, pp. C69–C69, Dec. 2017, doi:
45 10.1107/S2053273317095018.
46
47 [44] D. A. Keen, 'A comparison of various commonly used correlation functions for
48 describing total scattering', *J. Appl. Crystallogr.*, vol. 34, no. 2, pp. 172–177, Apr.
49
50
51
52
53
54
55
56
57
58
59
60

1
2
3 2001, doi: 10.1107/S0021889800019993.

- 4 [45] S. J. L. Billinge, 'The rise of the X-ray atomic pair distribution function method: a
5 series of fortunate events', *Philos. Trans. R. Soc. Math. Phys. Eng. Sci.*, vol. 377, no.
6 2147, p. 20180413, Jun. 2019, doi: 10.1098/rsta.2018.0413.
7
8
9
10
11
12
13
14
15
16
17
18
19
20
21
22
23
24
25
26
27
28
29
30
31
32
33
34
35
36
37
38
39
40
41
42
43
44
45
46
47
48
49
50
51
52
53
54
55
56
57
58
59
60